

The neuron-specific chromatin regulatory subunit BAF53b is necessary for synaptic plasticity and memory

Annie Vogel-Ciernia^{1,2}, Dina P Matheos^{1,2}, Ruth M Barrett³, Enikő A Kramár⁴, Soraya Azzawi^{1,2}, Yuncai Chen^{4,5}, Christophe N Magnan^{6,7}, Michael Zeller^{6,7}, Angelina Sylvain^{1,2}, Jakob Haettig^{1,2}, Yousheng Jia⁴, Anthony Tran^{1,2}, Richard Dang^{1,2}, Rebecca J Post^{1,2}, Meredith Chabrier¹, Alex H Babayan⁴, Jiang I Wu⁸, Gerald R Crabtree⁸, Pierre Baldi^{6,7}, Tallie Z Baram^{4,5}, Gary Lynch^{4,9} & Marcelo A Wood^{1,2}

Recent exome sequencing studies have implicated polymorphic Brg1-Associated Factor (BAF) complexes (mammalian SWI/SNF chromatin remodeling complexes) in several human intellectual disabilities and cognitive disorders. However, it is currently unknown how mutations in BAF complexes result in impaired cognitive function. Postmitotic neurons express a neuron-specific assembly, nBAF, characterized by the neuron-specific subunit BAF53b. Mice harboring selective genetic manipulations of BAF53b have severe defects in long-term memory and long-lasting forms of hippocampal synaptic plasticity. We rescued memory impairments in BAF53b mutant mice by reintroducing BAF53b in the adult hippocampus, which suggests a role for BAF53b beyond neuronal development. The defects in BAF53b mutant mice appeared to derive from alterations in gene expression that produce abnormal postsynaptic components, such as spine structure and function, and ultimately lead to deficits in synaptic plasticity. Our results provide new insight into the role of dominant mutations in subunits of BAF complexes in human intellectual and cognitive disorders.

It is generally accepted that gene expression is required for long-term memory formation; however, it remains unclear how gene expression is orchestrated by chromatin regulation during memory consolidation. Chromatin regulation via histone modification and DNA methylation is critical for controlling the gene expression that is required for normal memory processes¹, as demonstrated by animal studies and the association of these modifications with human disorders characterized by intellectual disability². Histone modification and DNA methylation represent two major mechanisms of chromatin regulation that are known to function intimately with ATP-dependent nucleosome remodeling, another major mechanism of chromatin regulation. Although much is known about the former mechanisms in memory formation, the role of nucleosome remodeling in memory processes and intellectual function remains poorly understood.

Nucleosome remodeling complexes are important for development, cancer and stem cell biology³. They utilize ATP hydrolysis to disrupt nucleosome-DNA contacts, move nucleosomes along DNA, and, from *in vitro* studies, are thought to remove or exchange nucleosomes. Nucleosome remodeling complexes are comprised of numerous subunits, and the exact compositions of different subunits are cell-type specific and developmentally regulated^{4–6}. A previous study identified the neuron-specific BAF (nBAF) complex, which contains a neuron-specific subunit, BAF53b. BAF53b is an actin-related protein,

with high homology to β -actin, and both BAF53b and nuclear β -actin are found as monomers in stoichiometric levels bound to Brg or Brm ATPases⁷ in the nBAF complex. These three proteins form the core of the nBAF complex and are responsible for targeting the Brg or Brm ATPases to specific gene promoters^{7,8}. BAF53b is unique among nucleosome remodeling complex subunits because it is neuron specific and is not found in any other nucleosome remodeling complex besides the nBAF complex^{6,8}. This unusual dedication of a subunit to a single neuronal complex makes BAF53b an ideal target for elucidating the role of the nBAF complex in learning and memory.

Homozygous deletion of *Baf53b* (also known as *Actl6b*) in mice is lethal. Neurons cultured from these mice have severe deficits in gene expression, dendritic arborization and synapse formation⁸. BAF53b begins to be expressed as neural progenitors exit mitosis and terminally differentiate into neurons^{6,9}. BAF53a, a homolog of BAF53b, is expressed in neural progenitors and is replaced by BAF53b following differentiation⁹. This switch is mediated by the repression of BAF53a expression via *miR-9** and *miR-124*, which are selectively expressed in postmitotic neurons¹⁰. Failure of miRNA-mediated repression of BAF53a results in decreased BAF53b expression and impaired dendritic outgrowth¹⁰. In contrast, expression of *miR-9** and *miR-124* in human fibroblasts induces their conversion into neurons, indicating that this overall mechanism is instructive in establishing neural cell

¹Department of Neurobiology and Behavior, University of California, Irvine, California, USA. ²Center for the Neurobiology of Learning and Memory, Irvine, California, USA. ³Oregon Health and Science University, Portland, Oregon, USA. ⁴Department of Anatomy and Neurobiology, University of California, Irvine, California, USA. ⁵Department of Pediatrics, University of California, Irvine, California, USA. ⁶Department of Computer Science, University of California, Irvine, California, USA. ⁷Institute for Genomics and Bioinformatics, University of California, Irvine, California, USA. ⁸Howard Hughes Medical Institute and Department of Developmental Biology, Stanford University School of Medicine, Stanford, California, USA. ⁹Department of Psychiatry and Human Behavior, University of California, Irvine, California, USA. Correspondence should be addressed to M.A.W. (mwood@uci.edu).

Received 29 December 2012; accepted 11 February 2013; published online 24 March 2013; doi:10.1038/nn.3359

fate¹¹. Given the highly coordinated regulation of BAF53b during neuronal differentiation and its role in synapse formation and dendritic arborization, it is important to understand the role of BAF53b and the nBAF complex in both the developing and adult brain.

Mutations in various subunits of nucleosome remodeling complexes have recently been implicated in human disorders characterized by intellectual disability. For example, dominant mutations in subunits of mammalian BAF complexes are implicated in Coffin-Siris and Nicolaides-Baraitser syndromes, both of which are associated with intellectual disability and specific digital abnormalities^{12–14}. In addition the nBAF component BAF250b (Arid1b) is mutated frequently in sporadic mental retardation^{12,13,15,16}, and BAF155, BAF170 and REST were found to be mutated in exome sequencing of sporadic autism¹⁷. These findings suggest that the BAF nucleosome remodeling complex regulates gene expression required for proper neuronal function, synaptic plasticity and memory processes. We asked whether the BAF complex has a role in memory processes that is distinct from its role in development. We directly addressed this by examining the role of a neuron-specific component of the BAF complex, BAF53b, in synaptic plasticity and memory.

RESULTS

Generation of BAF53b mutant mice

BAF53b is a neuron-specific stoichiometric component of BAF complexes that is not found in other nucleosome remodeling complexes⁸. To examine the role of BAF53b in long-term memory processes, we engineered transgenic mice that express a mutant form of murine BAF53b with a deletion of the hydrophobic domain (*BAF53b Δ H D* ; **Fig. 1a**). The rationale for this deletion is that the hydrophobic domain is predicted to enable protein-protein interactions with other subunits of nBAF complexes, and deletion of this domain in the non-neuronal homolog BAF53a has been shown to generate a dominant-negative form of BAF53a¹⁸. Given the high degree of homology between BAF53a and BAF53b, we predicted a similar dominant-negative effect of deleting the hydrophobic domain from BAF53b. The *BAF53b Δ H D* transgene (**Fig. 1a**) is driven by the *Camk2a* promoter¹⁹, which allows for restricted expression to forebrain excitatory neurons and postnatal development²⁰. Thus, we avoided developmental effects resulting from the known role of BAF53b in postmitotic

embryonic development. We developed two independent lines of *Camk2a-BAF53b Δ H D* mice. Both lines had normal brain morphology (**Supplementary Fig. 1a**), but were characterized by significantly different levels of transgene expression in hippocampal tissue (*BAF53b Δ H D* ^{high} and *BAF53b Δ H D* ^{low}, $P < 0.0001$; **Fig. 1b**), which is relevant to our hippocampus-dependent experiments. Wild-type BAF53b levels and localization were unaltered in the *BAF53b Δ H D* mice (**Fig. 1c** and **Supplementary Fig. 1b–d**).

In addition to the *BAF53b Δ H D* mice, we also examined BAF53b heterozygous null mice (*Baf53b^{+/-}*)⁸. *Baf53b^{-/-}* mice have a complete loss of *Baf53b* mRNA and protein, and die in the first two postnatal days⁸. Consistent with the exclusive expression of BAF53b in postmitotic neurons, they have no detectable defects outside of the nervous system⁸. *Baf53b^{+/-}* mice developed normally (**Supplementary Fig. 1**) and expressed approximately 50% as much *Baf53b* mRNA (**Fig. 1d**) and protein (**Fig. 1e**) as wild-type mice. *Baf53b* mRNA and protein expression in *Baf53b^{+/-}* mice was half of that in wild-type littermates both from home cage samples and after training (killed 30 min post object location memory (OLM) training; **Figs. 1d,e** and **2a**). Notably, there were no neuron-specific homologs of BAF53b that could compensate for its decreased expression. Thus, these results indicate that there is no compensation in expression in the *Baf53b^{+/-}* mice following behavior. In addition, both anxiety and motor function were found to be normal in *BAF53b Δ H D* and *Baf53b^{+/-}* mice as compared to wild-type controls (**Supplementary Fig. 2**), allowing us to examine memory processes in these mice.

BAF53b is required for long-term memory

To examine the role of BAF53b in memory, we tested *BAF53b Δ H D* and *Baf53b^{+/-}* mice for both long- and short-term OLM (**Fig. 2a**) and object recognition (ORM; **Fig. 2d**). Wild-type mice exhibited long-term OLM (as measured by preference for the novel location over the familiar location and calculated as the discrimination index; **Fig. 2b,c**). However, both *BAF53b Δ H D* ^{high} and *BAF53b Δ H D* ^{low} mice exhibited significantly reduced discrimination indices compared with wild-type littermates ($P < 0.01$; **Fig. 2b**). Similar to the *BAF53b Δ H D* lines, *Baf53b^{+/-}* mice also exhibited significant deficits in long-term OLM ($P < 0.05$; **Fig. 2c**). In contrast with the long-term memory deficits, short-term OLM

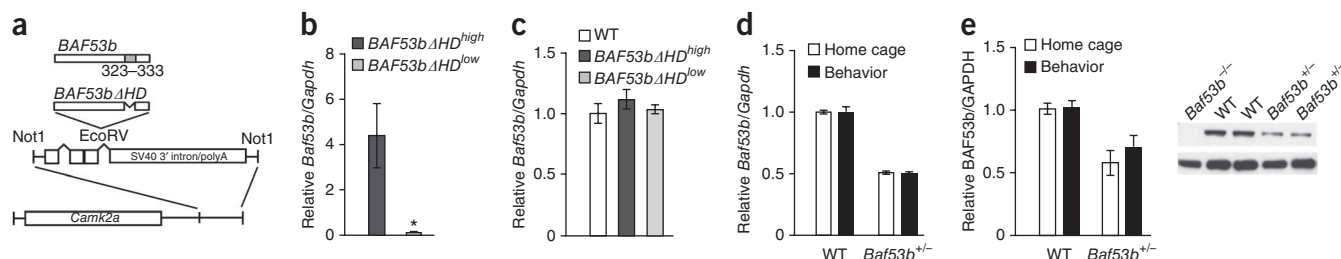
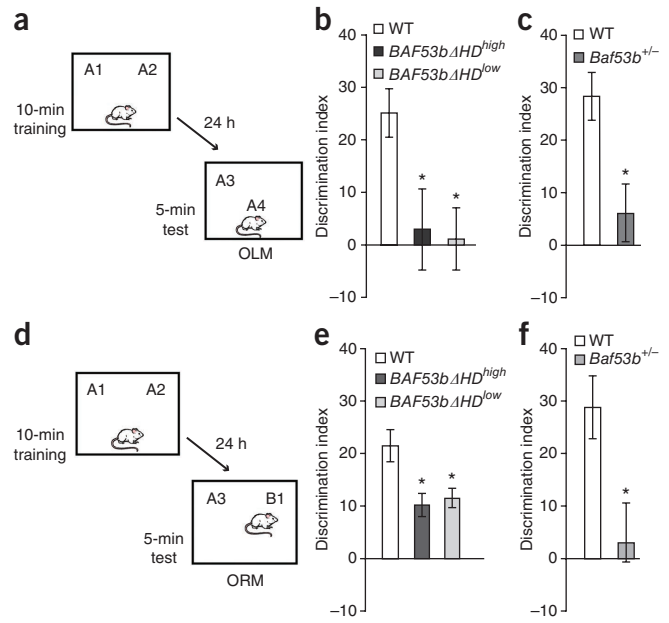


Figure 1 Characterization of *BAF53b Δ H D* and *Baf53b^{+/-}* mice. **(a)** Wild-type *Baf53b* is diagrammed with the hydrophobic domain shown in gray. In the *BAF53b Δ H D* construct, amino acids 323–333 in the hydrophobic domain were deleted. The *BAF53b Δ H D* mutant sequence was cloned into a separate vector containing intron and exon sequences with splice sites and the SV40 intron and polyadenylation signal, which was then cloned downstream of the 8.5-kb mouse *Camk2a* promoter. This construct was used to generate the *BAF53b Δ H D* transgenic mice. **(b)** Quantitative reverse transcription PCR (qRT-PCR) was performed with transgene-specific primers to measure transgene expression in dorsal hippocampus of two independently derived lines of *BAF53b Δ H D* mice. We identified two significantly different lines (Mann-Whitney $U(18) = 0.00$, $P < 0.0001$): *BAF53b Δ H D* ^{low} ($n = 10$) and *BAF53b Δ H D* ^{high} ($n = 10$) (2 of 12 founder lines). **(c)** Wild-type (WT) BAF53b expression in the dorsal hippocampus of *BAF53b Δ H D* ^{high} ($n = 10$) and *BAF53b Δ H D* ^{low} ($n = 11$) mice was not significantly different (Kruskal-Wallis $H_{2,33} = 4.03$, $P = 0.13$) between mutant mice and wild-type littermates ($n = 15$). **(d)** qRT-PCR revealed that wild-type *Baf53b* expression in the dorsal hippocampus of *Baf53b^{+/-}* mice ($n = 13$) was significantly (two-way ANOVA main effect of genotype, $F_{1,18} = 17.87$, $P < 0.001$) reduced compared with wild-type littermates ($n = 8$). There was no effect of behavior ($F_{1,18} = 0.81$, $P = 0.38$) or interaction ($F_{1,18} = 0.40$, $P = 0.53$). **(e)** Western blot analysis revealed that BAF53b protein expression in dorsal hippocampus of *Baf53b^{+/-}* mice ($n = 13$) was significantly (two-way ANOVA main effect of genotype, $F_{1,17} = 345.0$, $P < 0.0001$) reduced compared with wild-type littermates ($n = 9$). There was no effect of behavior ($F_{1,17} = 0.05$, $P = 0.82$) or interaction ($F_{1,17} = 0.03$, $P = 0.85$). * $P < 0.05$, n values refer to number of mice. Data are presented as mean \pm s.e.m.

Figure 2 *BAF53b* Δ *HD* and *Baf53b*^{+/-} mice have impaired long-term memory.

(a) Mice received 10 min of training in an environment with two identical objects and received a retention test 24 h later in which one object was moved to a new location (OLM). (b) *BAF53b* Δ *HD*^{high} ($n = 9$) and *BAF53b* Δ *HD*^{low} ($n = 13$) mice exhibited a significant 24-h long-term OLM deficit (ANOVA, $F_{2,34} = 5.79$, $P < 0.01$) in a hippocampus-dependent task as compared with wild-type littermates ($n = 15$) and were not significantly different from zero (*BAF53b* Δ *HD*^{high}, t test $t_8 = 0.39$, $P = 0.71$; *BAF53b* Δ *HD*^{low}, t test $t_{12} = 0.19$, $P = 0.85$). There were no significant differences in total exploration time between the groups during testing (ANOVA, $F_{2,34} = 0.45$, $P = 0.64$) or training (ANOVA, $F_{2,34} = 1.13$, $P = 0.33$). (c) *Baf53b*^{+/-} mice ($n = 16$) exhibited impaired long-term OLM compared with wild-type mice ($n = 6$, t test $t_{20} = 2.35$, $P < 0.05$). There was no difference in overall exploration time between the groups at training (t test $t_{20} = 0.40$, $P = 0.70$) or testing (t test $t_{20} = 0.95$, $P = 0.35$). (d) Mice received 10 min of training in an environment with two identical objects and received a retention test 24 h later in which one object was replaced with a novel one (ORM). (e) In a hippocampus-independent object recognition task, *BAF53b* Δ *HD*^{high} ($n = 12$) and *BAF53b* Δ *HD*^{low} ($n = 11$) mice exhibited significant ORM deficits as compared with wild-type mice ($n = 18$, Kruskal-Wallis $H_{2,38} = 10.72$, $P < 0.01$; *BAF53b* Δ *HD*^{high}, $t_{11} = 13.06$, $P < 0.05$; *BAF53b* Δ *HD*^{low}, $t_{10} = 11.43$, $P < 0.05$; Dunn's *post hoc* tests). There were no differences in total exploration time between the groups at training (Kruskal-Wallis $H_{2,38} = 0.61$, $P = 0.98$) or testing (ANOVA $F_{2,30} = 2.53$, $P = 0.09$). (f) *Baf53b*^{+/-} mice ($n = 9$) exhibited impaired long-term ORM compared with wild-type mice ($n = 10$; t test $t_{17} = 2.88$, $P < 0.05$). There was no difference in the overall exploration time between the groups at training (t test $t_{17} = 0.60$, $P = 0.56$) or testing (t test $t_{17} = 0.36$, $P = 0.72$). * $P < 0.05$, n values refer to number of mice. Data are presented as mean \pm s.e.m.



(tested at 90 min) was normal in *BAF53b* Δ *HD* mice (Supplementary Fig. 3b) and *Baf53b*^{+/-} mice (Supplementary Fig. 3c) as compared to wild-type littermates. Deficits in long-term memory formation were also found in the object recognition task (Fig. 2d). Wild-type mice exhibited normal long-term ORM (as measured by preference for the novel object over the familiar object and calculated as the discrimination index). Both the *BAF53b* Δ *HD*^{high} and *BAF53b* Δ *HD*^{low} mice had significantly reduced discrimination indices compared with wild-type littermates ($P < 0.05$; Fig. 2e). *Baf53b*^{+/-} mice also showed significant long-term ORM deficits ($P < 0.05$; Fig. 2f). In contrast, short-term ORM (tested at 90 min) was normal in *BAF53b* Δ *HD* mice (Supplementary Fig. 3e) and *Baf53b*^{+/-} mice as compared to wild-type littermates (Supplementary Fig. 3f).

Together, these results suggest that BAF53b is critical for long-term memory formation. Notably, all of the BAF53b mutant mice (*BAF53b* Δ *HD* and *Baf53b*^{+/-}) had normal short-term memory, indicating that they can perform these tasks and that their deficits at 24 h are the results of a failure of learning and memory, rather than performance. These results also support the hypothesis that BAF53b is involved in regulating gene expression required for long-term memory, as short-term memory in these tasks was transcription independent.

In addition to ORM and OLM tasks, we examined long-term memory for contextual and cued fear conditioning in *BAF53b* Δ *HD*^{low} and *Baf53b*^{+/-} mice. Both lines exhibited normal response to shock, as measured by an increase in velocity in response to the shock (Fig. 3a,d). *BAF53b* Δ *HD*^{low} mice exhibited a significant decrease in freezing in a 24-h retention test, indicating impaired long-term memory for contextual fear ($P < 0.05$; Fig. 3b). In contrast, long-term memory for cued fear was normal in *BAF53b* Δ *HD*^{low} mice as compared to wild-type littermates in a 24-h retention test (Fig. 3c). Similar results were observed in *Baf53b*^{+/-} mice, which exhibited a significant decrease in freezing in the conditioned context in a 24-h retention test, indicating impaired long-term memory for contextual fear ($P < 0.05$; Fig. 3e). In contrast, long-term memory for cued fear was normal in *Baf53b*^{+/-} mice as compared to

wild-type littermates in a 24-h retention test (Fig. 3f). Together, these results suggest that BAF53b is involved in long-term memory for contextual fear, but perhaps not in cued fear memory. Because contextual fear conditioning is hippocampus dependent, whereas cued fear conditioning is hippocampus independent, these results also suggest that the hippocampus may be more sensitive to alterations in BAF53b.

Reintroducing BAF53b into dorsal hippocampus rescues OLM

To assess whether BAF53b is sufficient for long-term memory formation in the hippocampus, we reintroduced wild-type BAF53b into the dorsal hippocampus of adult *Baf53b*^{+/-} mice and wild-type littermates using adeno-associated virus (AAV). AAV expressing BAF53b (AAV-*Baf53b*) or GFP (AAV-*hrGFP*) was surgically delivered into dorsal hippocampus 14 d before behavior. AAV-*Baf53b* was robustly expressed in the dorsal hippocampus and BAF53b protein levels in the *Baf53b*^{+/-} mice treated with AAV-*Baf53b* were increased to wild-type levels in CA1 (Fig. 4a,b). Notably, all four groups (wild-type AAV-*hrGFP*, *Baf53b*^{+/-} AAV-*hrGFP*, wild-type AAV-*Baf53b*, *Baf53b*^{+/-} AAV-*Baf53b*) showed normal motor function and anxiety (Supplementary Fig. 2). All four groups were tested for long-term OLM (hippocampal dependent) followed by long-term ORM (in a novel context with different objects; hippocampal independent) (Fig. 4c). Wild-type AAV-*hrGFP*-treated mice showed a robust preference for the displaced object indicating long-term OLM (Fig. 4d). *Baf53b*^{+/-} AAV-*hrGFP*-treated mice showed significantly impaired OLM, replicating our previous findings ($P < 0.05$; Fig. 2c). Wild-type AAV-*Baf53b*-treated mice also showed a robust preference for the displaced object, similar to wild-type AAV-*hrGFP*-treated mice. Notably, *Baf53b*^{+/-} mice treated with AAV-*Baf53b* showed a robust preference for the displaced object that was indistinguishable from that of wild-type mice, demonstrating a complete rescue of long-term OLM formation (Fig. 4d). These findings indicate that the memory deficits observed in the *Baf53b*^{+/-} mice (Figs. 2c and 4d) are a result of BAF53b having a role in regulating gene expression in the adult brain and not of its role in development.

Figure 3 *BAF53bΔHD^{low}* and *Baf53b^{+/-}* mice have impairments in long-term memory for contextual fear, but normal cued fear memory.

(a) During contextual fear training, velocity (cm s^{-1}) did not differ between *BAF53bΔHD^{low}* ($n = 10$) and wild-type ($n = 9$) mice for the 5 s before shock (pre-shock) or during the shock (shock) (repeated-measures ANOVA $F_{1,17} = 234.2$, $P < 0.0001$; Bonferroni *post hoc t* test pre-shock versus post shock: wild type, t test $t_8 = 10.09$, $P < 0.001$; *BAF53bΔHD^{low}*, t test $t_9 = 11.60$, $P < 0.001$) and there was no effect of genotype (ANOVA $F_{1,17} = 0.44$, $P = 0.51$) or interaction ($F_{1,17} = 0.44$, $P = 0.51$).

(b) Mice were tested in the conditioned context 24 h after conditioning.

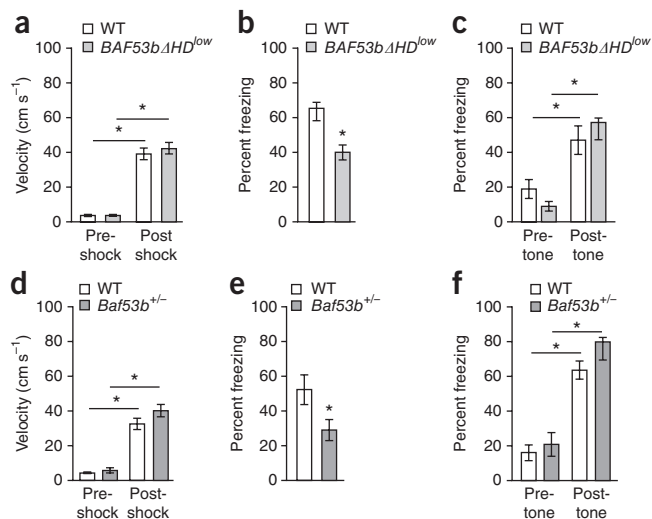
BAF53bΔHD^{low} mice froze significantly less than wild-type mice (t test $t_{17} = 3.46$, $P < 0.05$). At test, there was a significant main effect of sex (ANOVA $F_{1,15} = 12.39$, $P = 0.003$), but no interaction with genotype ($F_{1,15} = 0.03$, $P = 0.86$), with *BAF53bΔHD^{low}* males freezing more than females (Bonferroni *post hoc t* test $t_9 = 2.58$, $P < 0.05$) and a similar (but not significant) trend in wild type (Bonferroni *post hoc t* test $t_8 = 2.40$, $P > 0.05$).

(c) 24-h memory test for cued fear conditioning (test in novel context). Both groups exhibited similar levels of freezing before tone onset (pre-tone) and after tone onset (post-tone) (repeated-measures ANOVA $F_{1,16} = 0.98$, $P = 0.77$), with a significant increase in freezing following tone onset in both groups ($F_{1,16} = 38.21$, $P < 0.0001$, Bonferroni *post hoc t* test pre-tone versus post-tone: wild type, $t_7 = 3.21$, $P < 0.05$, $n = 8$; *BAF53bΔHD^{low}*, $t_9 = 5.68$, $P < 0.001$, $n = 10$).

(d) *Baf53b^{+/-}* mice ($n = 9$) had a normal response to the shock during contextual fear training compared to wild-type littermates ($n = 8$), with a significant increase in velocity following shock for both groups (repeated-measures ANOVA $F_{1,15} = 183.3$, $P < 0.0001$; Bonferroni *post hoc t* test pre-shock versus post shock: wild type, $t_7 = 8.38$, $P < 0.001$; *Baf53b^{+/-}*, $t_8 = 10.85$, $P < 0.001$), and no effect of genotype ($F_{1,15} = 2.57$, $P = 0.13$) or interaction ($F_{1,15} = 1.80$, $P = 0.20$).

(e) *Baf53b^{+/-}* mice froze significantly less than wild type at the 24-h long-term contextual fear memory test (t test $t_{15} = 2.25$, $P < 0.05$).

(f) 24-h memory test for cued fear conditioning (test in novel context). Both groups exhibited similar levels of freezing before tone onset (pre-tone) and after tone onset (post-tone) (repeated-measures ANOVA $F_{1,22} = 0.53$, $P = 0.48$) with a significant increase in freezing following tone onset in both groups (ANOVA $F_{1,22} = 63.29$, $P < 0.0001$; Bonferroni *post hoc t* test pre-tone versus post-tone: wild type, $t_{11} = 6.56$, $P < 0.001$, $n = 12$; *Baf53b^{+/-}*, $t_{11} = 4.69$, $P < 0.001$, $n = 12$). * $P < 0.05$, n values refer to number of mice. Data are presented as mean \pm s.e.m.



To examine the specificity of the long-term memory rescue, we tested the same animals on the hippocampal-independent long-term ORM task (Fig. 4e). Similar to our previous findings with the *Baf53b^{+/-}* mice (Fig. 2f), wild-type AAV-*hrGFP*-treated mice showed a robust preference for the novel object, indicating long-term ORM. The *Baf53b^{+/-}* mice treated with AAV-*hrGFP* showed significantly impaired ORM, replicating our previous findings ($P < 0.05$; Fig. 2f). Wild-type mice treated with AAV-*Baf53b* also showed long-term ORM; however, in the ORM task, the *Baf53b^{+/-}* mice treated with AAV-*Baf53b* failed to show a preference for the novel object ($P < 0.05$; Fig. 4e). Given the spatially restricted viral expression in dorsal hippocampus of the *Baf53b^{+/-}* AAV-*Baf53b*-treated mice, the failure to rescue a hippocampal-independent memory task (ORM) demonstrates specificity for the OLM rescue and not a global change in brain state or processing. Overall, these findings provide strong evidence that BAF53b is critical for long-term memory formation in adult mice.

LTP fails to stabilize in slices from BAF53b mutant mice

To assess the potential contributions of BAF53b in synaptic plasticity, a cellular mechanism that is thought to underlie memory processes, we examined long-term potentiation (LTP) in acute hippocampal slices from *BAF53bΔHD* and *Baf53b^{+/-}* mice. Wild-type slices were tested concurrently with a subset of cases for each of the three experimental groups. Theta burst stimulation (TBS) was delivered to one input in CA1c to stimulate a single collection of Schaffer-commissural fibers while a second input delivering only low-frequency (three pulses per min) stimulation (LFS) in CA1a was used to monitor slice stability. We detected no changes over time in the excitatory postsynaptic potential (EPSP) slopes elicited by LFS in any of the slice groups (Supplementary Fig. 4a).

A single train of ten theta bursts, which have shown to be well above the threshold (number of bursts) needed to induce LTP^{21,22}, produced a robust and immediate potentiation in wild-type slices that steadily

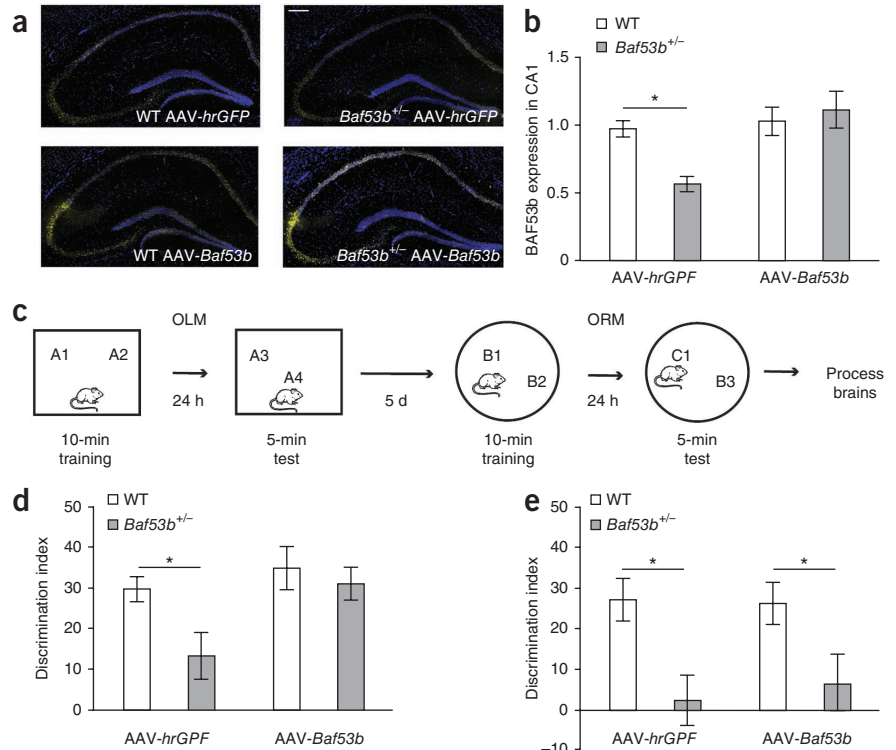
decayed over 10 min to a plateau level that was approximately 60% above the pre-TBS baseline (the mean (\pm s.e.m.) LTP for minutes 50–60 post-TBS was $59 \pm 4\%$). Hippocampal slices prepared from *Baf53b^{+/-}* mice exhibited a very different pattern: short-term potentiation (STP) was not measurably different from wild-type values, but the enhanced responses failed to stabilize and instead gradually fell back to baseline (Fig. 5a). Percent facilitation for the last 10 min of the 1-h post-TBS session was $14 \pm 6\%$ ($P < 0.0001$ versus wild type).

Initial studies with slices from *BAF53bΔHD^{low}* mice did not detect any abnormalities in the LTP elicited by ten theta bursts from that obtained from wild-type mice (Fig. 5b). We therefore repeated the experiment using trains of five theta bursts, a protocol that is closer to the threshold for eliciting stable LTP in mice. A marked defect was found under these conditions. Five bursts delivered to wild-type slices produced STP and LTP effects comparable to those induced by ten bursts; slices from the *BAF53bΔHD^{low}* mice exhibited normal STP, but potentiation failed to stabilize and decayed over the next hour to levels that were markedly lower than those recorded for the controls ($P < 0.001$ at 50–60 min post-TBS; Fig. 5c). These results suggest that low expression of the BAF53bΔHD mutant protein is sufficient to markedly impair the machinery required to consolidate LTP and that this impairment can be overcome by supra-threshold stimulation.

We next tested whether the higher expression of mutant BAF53bΔHD in *BAF53bΔHD^{high}* mice would reproduce the total loss of LTP found in the *Baf53b^{+/-}* mice. Slices prepared from *BAF53bΔHD^{high}* mice had unexpected responses to ten theta bursts. Initial potentiation was greatly amplified (facilitation at 2 min post-TBS was $239 \pm 31\%$ compared with $156 \pm 10\%$ for wild types; $P = 0.003$), but then showed a failure to stabilize similar to the *BAF53bΔHD^{low}* and *Baf53b^{+/-}* mice (Fig. 5d). Collectively, these findings suggest that BAF53b is required for consolidation of lasting changes in synaptic strength and that somewhat lower levels are needed to maintain STP in normal boundaries.

Figure 4 Hippocampal AAV-*Baf53b* rescues OLM, but not ORM, deficits in *Baf53b*^{+/-} mice.

(a) Representative images of BAF53b (yellow) expression in wild-type and *Baf53b*^{+/-} mice treated with AAV-*hrGFP* or AAV-*Baf53b*. Nuclei (blue) were counterstained with DAPI. Scale bar represents 200 μ m. (b) Mean intensity of BAF53b immunofluorescence from CA1 cell layer normalized to background (corpus colossum). There was a complete return of BAF53b expression in CA1 of *Baf53b*^{+/-} mice compared with wild-type levels (ANOVA, no main effect of genotype, $F_{1,38} = 2.23$, $P = 0.14$; main effect of virus, $F_{1,38} = 8.14$, $P < 0.01$; significant interaction, $F_{1,38} = 5.34$, $P < 0.05$) (Bonferroni *post hoc* *t* test wild-type versus *Baf53b*^{+/-} mice: AAV-*hrGFP*, *t* test $t_{16} = 2.5$, $P < 0.05$; AAV-*Baf53b*, *t* test $t_{22} = 0.62$, $P > 0.05$; wild type AAV-*hrGFP*, $n = 10$; wild type AAV-*Baf53b*, $n = 12$; *Baf53b*^{+/-} AAV-*hrGFP*, $n = 9$; *Baf53b*^{+/-} AAV-*Baf53b*, $n = 12$). (c) Schematic of behavioral testing. Mice were first trained and tested for OLM. Following a 5-d rest period, mice were habituated to a novel context and then underwent ORM training and testing. (d) Long-term OLM (24 h). There was a complete rescue of OLM in *Baf53b*^{+/-} mice with AAV-*Baf53b* (two-way ANOVA; main effect genotype, $F_{1,40} = 4.49$, $P < 0.05$; main effect of virus, $F_{1,40} = 6.04$, $P < 0.05$; no interaction, $F_{1,40} = 1.76$, $P = 0.19$; Bonferroni *post hoc* *t* test wild-type versus *Baf53b*^{+/-} mice: AAV-*hrGFP*, *t* test $t_{18} = 2.33$, $P < 0.05$; AAV-*Baf53b*, *t* test $t_{22} = 0.59$, $P > 0.05$). There was no difference between any of the groups for total exploration at training (two-way ANOVA; no effect of genotype, $F_{1,40} = 3.56$, $P = 0.07$; no effect of virus, $F_{1,40} = 0.02$, $P = 0.90$; no interaction, $F_{1,40} = 0.63$, $P = 0.43$) or testing (two-way ANOVA; no effect of genotype, $F_{1,40} = 0.29$, $P = 0.59$; no effect of virus, $F_{1,40} = 0.53$, $P = 0.47$; no interaction, $F_{1,40} = 4.02$, $P = 0.05$; wild type AAV-*hrGFP*, $n = 10$; wild type AAV-*Baf53b*, $n = 12$; *Baf53b*^{+/-} AAV-*hrGFP*, $n = 10$; *Baf53b*^{+/-} AAV-*Baf53b*, $n = 12$). (e) Long-term ORM (24 h). There was no rescue of ORM in *Baf53b*^{+/-} mice with AAV-*Baf53b* expression in dorsal hippocampus (two-way ANOVA; main effect genotype, $F_{1,33} = 12.79$, $P < 0.01$; no main effect of virus, $F_{1,33} = 0.08$, $P = 0.77$; no interaction, $F_{1,33} = 0.16$, $P = 0.69$; Bonferroni *post hoc* *t* test wild-type versus *Baf53b*^{+/-} mice: AAV-*hrGFP*, *t* test $t_{14} = 2.63$, $P < 0.05$; AAV-*Baf53b*, *t* test $t_{19} = 2.42$, $P < 0.05$). There was no difference between any of the groups for total exploration at training (two-way ANOVA; no effect of genotype, $F_{1,33} = 1.08$, $P = 0.31$; no effect of virus, $F_{1,33} = 2.85$, $P = 0.10$; no interaction, $F_{1,33} = 0.04$, $P = 0.84$) or testing (two-way ANOVA; no effect of genotype, $F_{1,33} = 4.13$, $P = 0.05$; no effect of virus, $F_{1,33} = 1.78$, $P = 0.19$; no interaction, $F_{1,33} = 0.51$, $P = 0.48$) (wild type AAV-*hrGFP*, $n = 7$; wild type AAV-*Baf53b*, $n = 10$; *Baf53b*^{+/-} AAV-*hrGFP*, $n = 9$; *Baf53b*^{+/-} AAV-*Baf53b*, $n = 11$). * $P < 0.05$, n values refer to number of mice. Data are presented as mean \pm s.e.m.



We then investigated which aspects of the complex series of events leading to induction, expression and consolidation of LTP are negatively affected by manipulations of BAF53b by examining conventional measures of transmission and the responses to theta bursts. Input-output curves (number of axons stimulated / magnitude of postsynaptic response) were comparable for wild-type and either *Baf53b*^{+/-} or *BAF53bΔHD*^{low} mice, but there was a marked depression of the curve in the *BAF53bΔHD*^{high} mice (Fig. 5e). The most straightforward interpretation of these results is that high expression of the *BAF53bΔHD* mutation affects axon excitability. Consistent with this idea, the slope of the relationship between stimulation current and the amplitude of the fiber volley, a measure of the number of responsive axons, was reduced for the *BAF53bΔHD*^{high} slices, but not for the other two genotypes, relative to wild type (Fig. 5f). We then tested the genotypes for differences in transmitter release kinetics using paired pulse facilitation, a measure of the extent to which release triggered by a single stimulation pulse increases release by a slightly delayed second pulse. The *Baf53b*^{+/-} and *BAF53bΔHD*^{low} slices did not differ from wild-type slices, but the *BAF53bΔHD*^{high} slices were enhanced ($P < 0.0001$; Fig. 5g). However, whole-cell recording revealed that the frequency and magnitude of miniature EPSPs in the *BAF53bΔHD*^{high} slices were comparable to wild-type values (Fig. 5h). In sum, *BAF53bΔHD*^{high} slices were characterized by depressed axon

excitability and exaggerated transmitter mobilization while spontaneous release and associated postsynaptic receptor responses appeared to be normal. The *Baf53b*^{+/-} slices and *BAF53bΔHD*^{low} cases were comparable to controls on all tests of baseline physiology.

The above measures suggest that the failure of LTP consolidation in the *Baf53b*^{+/-} and *BAF53bΔHD*^{low} mice cannot be attributed to presynaptic variables. We therefore examined the magnitude and within-train facilitation of the postsynaptic responses to theta bursts in these two groups. This analysis uncovered no differences between the two genotypes and wild-type slices (Supplementary Fig. 4b,c). Thus, it appears that the loss of LTP in the mutants involves factors that operate after induction and initial expression of potentiation, a conclusion that is consistent with our observation that STP was unaffected in these mice (Fig. 5a-c).

The *Baf53b*^{+/-} mice showed robust failure in the expression of LTP. Thus, we wanted to determine whether the mice showed deficits in activity-induced actin signaling. TBS stimulation activates actin regulatory pathways and alters synapse morphology in the same dendritic spines, as shown by a TBS-induced increase in spines containing phosphorylated p21-activated kinase (PAK) or its downstream target Cofilin²³. Using wide-field deconvolution microscopy and immunofluorescent labeling, we found that phosphorylated Cofilin (pCofilin) had punctate labeling in stratum radiatum of CA1 and colocalized

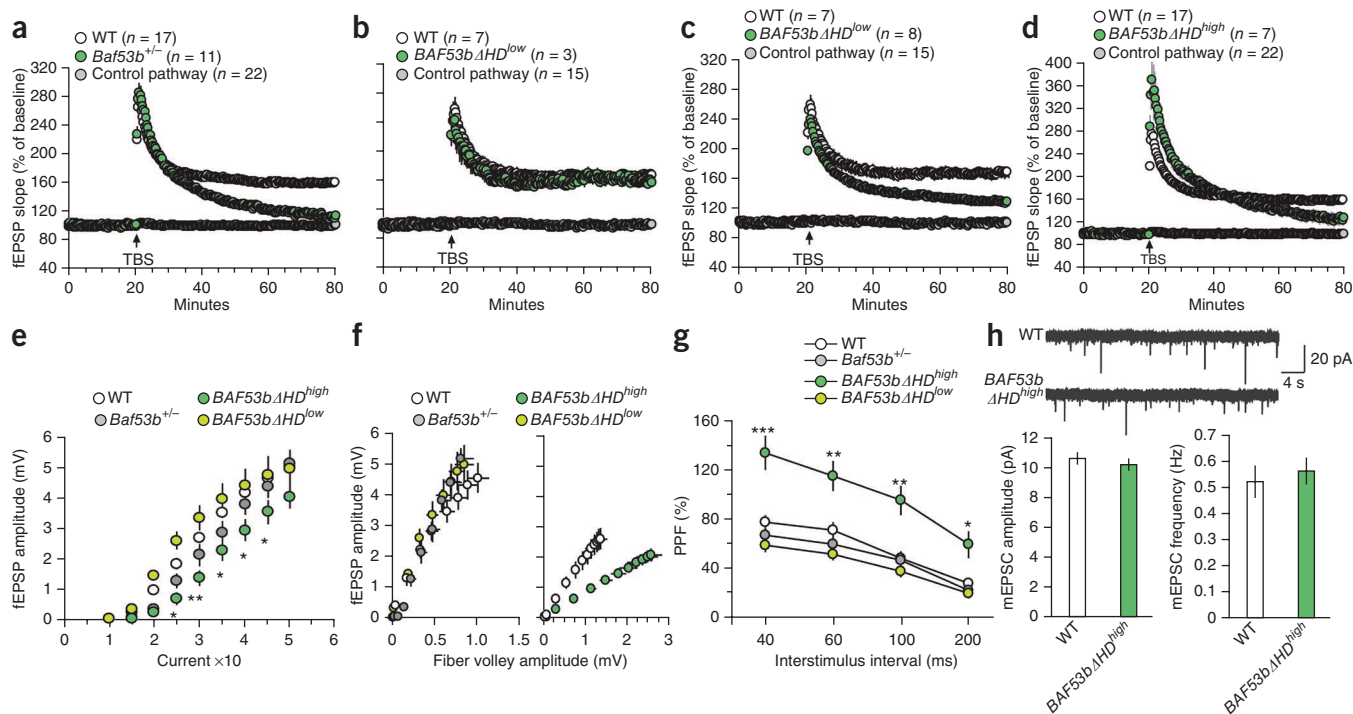


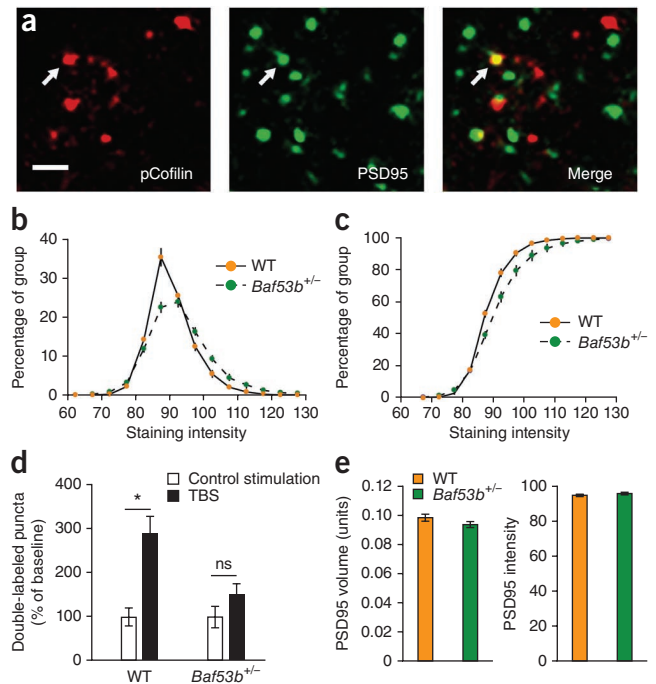
Figure 5 *BAF53b* Δ *HD* and *Baf53b*^{+/-} mice have disrupted LTP in hippocampal slices. (a,b) Simultaneous recordings of field EPSP (fEPSP) slope from slices receiving baseline stimulation (control, three pulses per min) and ten theta bursts (TBS) for wild-type and *Baf53b*^{+/-} slices. *Baf53b*^{+/-} slices failed to maintain stable LTP (average for last 5 min; *t* test $t_{26} = 6.48$, $P < 0.0001$). *BAF53b* Δ *HD*^{low} slices produced stable potentiation similar to wild-type slices ($t_8 = 0.30$, $P = 0.79$). (c) LTP induced with five theta bursts delivered to one of the two stimulation electrodes (control received baseline stimulation) produced stable potentiation in wild-type slices, but not in *BAF53b* Δ *HD*^{low} slices ($t_{13} = 3.77$, $P < 0.01$). (d) Simultaneous recordings of fEPSP slope in slices receiving low-frequency stimulation and ten theta bursts in wild-type and *BAF53b* Δ *HD*^{high} slices ($t_{22} = 3.49$, $P < 0.01$). (e) Input-output curves measuring the magnitude of the fEPSP response across a range of stimulation currents (10–50 μ A) was comparable between *Baf53b*^{+/-}, *BAF53b* Δ *HD*^{low} and wild-type slices, but not *BAF53b* Δ *HD*^{high} slices (two-way repeated ANOVA; main effect of genotype, $F_{3,35} = 4.47$, $P < 0.01$; main effect of time, $F_{8,35} = 246.7$, $P < 0.0001$; significant interaction, $F_{24,35} = 2.01$, $P < 0.005$). For each stimulation current, Bonferroni *post hoc t* test for wild-type ($n = 20$) versus *Baf53b*^{+/-} slices ($n = 6$), wild-type ($n = 20$) versus *BAF53b* Δ *HD*^{high} slices ($n = 7$), and wild-type ($n = 20$) versus *BAF53b* Δ *HD*^{low} slices ($n = 6$) are given in **Supplementary Figure 4**. * $P < 0.05$, ** $P < 0.01$. (f) Input-output curves comparing amplitudes of the presynaptic fiber volley to the fEPSP amplitude across a range of stimulation currents. Left, input-output curves were not different between *Baf53b*^{+/-} ($n = 6$), *BAF53b* Δ *HD*^{low} ($n = 6$) and wild-type mice ($n = 6$) (ANOVA $F_{2,15} = 1.04$, $P = 0.38$). Right, the slope was significantly reduced in the input-output curve produced from *BAF53b* Δ *HD*^{high} ($n = 12$) relative to wild type slices ($n = 12$) bathed in artificial cerebrospinal fluid containing 3 mM Mg^{2+} and 1 mM Ca^{2+} (Mann-Whitney *U* (22) = 3.00, $P < 0.0001$). (g) Paired pulse facilitation (PPF) of the initial slope of the synaptic response was comparable (40-, 60-, 100- and 200-ms inter-pulse intervals) in slices from *Baf53b*^{+/-} ($n = 9$), *BAF53b* Δ *HD*^{low} ($n = 7$) and wild-type mice ($n = 14$), but not in *BAF53b* Δ *HD*^{high} mice ($n = 6$) (two-way repeated ANOVA; main effect of genotype, $F_{3,32} = 11.60$, $P < 0.0001$; main effect of interval, $F_{3,32} = 192.6$, $P < 0.0001$; significant interaction, $F_{9,32} = 3.31$, $P < 0.005$; see Bonferroni *post hoc* comparisons in **Supplementary Fig. 4**). *** $P < 0.001$. (h) Top, sample traces of miniature excitatory postsynaptic currents (mEPSCs) recorded from *BAF53b* Δ *HD*^{high} ($n = 14$) and wild-type ($n = 15$) neurons. Bottom, there were no differences in mEPSCs from *BAF53b* Δ *HD*^{high} and wild-type neurons for the amplitude (left, $t_{27} = 0.75$, $P = 0.46$) and frequency (right, $t_{27} = 0.52$, $P = 0.61$). Data are presented as mean \pm s.e.m.

with PSD95, a marker of excitatory synapses (Fig. 6a). Quantification revealed that the intensity profiles of pCofilin puncta colocalized with PSD95 were right shifted in the *Baf53b*^{+/-} mice, indicating an increase in more intensely labeled puncta (Fig. 6b,c). pCofilin has been shown to peak 7 min post-TBS²⁴. Thus, we examined pCofilin at this time point in *Baf53b*^{+/-} mice and wild-type littermates. Wild-type mice showed a clear TBS-induced increase in the number of densely labeled pCofilin puncta colocalized to PSD95 7 minutes after TBS, whereas the *Baf53b*^{+/-} mice did not show a TBS-induced increase in double-labeled puncta (Fig. 6d). This difference was not a result of any changes detected in PSD95 volumes or intensities (Fig. 6e), suggesting that the postsynaptic terminal between the two groups is structurally similar.

In view of the localization of the marked functional synaptic deficits to the postsynaptic compartment in *BAF53b* Δ *HD*^{high} mice (Fig. 5), we more closely assessed the number and structure of dendritic spines, the sites of postsynaptic elements. Crossing the *BAF53b* Δ *HD*^{high} mice

with a mouse line expressing YFP under the *Thy1* promoter in pyramidal cells, we confirmed the overall normal anatomy of the hippocampus (Supplementary Fig. 5a). We then analyzed the spectrum of spine types (Supplementary Fig. 5b) encompassing subpopulations of thin, stubby and mushroom-like spines^{25–27}. The overall density of dendritic spines was modestly lower in *BAF53b* Δ *HD*^{high} mice than in wild-type mice (Supplementary Fig. 5f). However, a significant decrease in thin spines was apparent in the assessed CA1 pyramidal cells, including both main (stem) and oblique apical branches, resulting in an abnormally low ratio of thin to mushroom spines ($P < 0.01$; Supplementary Fig. 5c–e). The already abnormal distribution of dendritic spine subpopulations in juvenile *BAF53b* Δ *HD*^{high} mice is consistent with the problems in synaptic function and plasticity found in these mice. Together with our immunostaining data (Fig. 6), these results indicate that *BAF53b* may have roles in both spine morphology and structure, as well as synaptic events, depending on the type of *Baf53b* mutation.

Figure 6 TBS-induced phosphorylation of Cofilin is altered in *Baf53b*^{+/-} mice. Adult mouse hippocampal slices were stimulated electrophysiologically and immunolabeled. (a) Immunocytochemical labeling revealed colocalization of pCofilin- (red) and PSD95-immunoreactive puncta (green). Scale bar represents 2.5 μ m. (b) Distribution of double-labeled pCofilin intensities. *Baf53b*^{+/-} mice had a different baseline distribution than wild type, with an increase in the more intensely labeled puncta. (c) Cumulative probability distributions revealed that the *Baf53b*^{+/-} mice had curves that were shifted to the right relative to their wild-type counterparts, thus favoring the more intense puncta. (d) Bar graph shows values of double-labeled puncta 7 min after control stimulation (three pulses per min) or ten theta bursts (TBS), with values normalized to respective control stimulation group (ANOVA; main effect of stimulation, $F_{1,25} = 14.92$, $P < 0.005$; main effect of genotype, $F_{1,25} = 5.13$, $P < 0.05$; significant interaction, $F_{1,25} = 5.11$, $P < 0.05$; Bonferroni corrected *post hoc t* test control versus TBS: wild-type, $t_{12} = 4.24$, $P < 0.001$; *Baf53b*^{+/-}, $t_{13} = 1.16$, $P > 0.05$; wild-type control, $n = 8$; wild-type TBS, $n = 8$; *Baf53b*^{+/-} control, $n = 7$; *Baf53b*^{+/-} TBS, $n = 8$). (e) Left, quantification of the mean volumes of PSD95-immunoreactive puncta that were colocalized with pCofilin for *Baf53b*^{+/-} mice ($n = 15$) and wild-type littermates ($n = 16$) (*t* test $t_{29} = 1.39$, $P = 0.19$). Right, mean intensities of PSD95-labeled elements also revealed no difference between the *Baf53b*^{+/-} mice ($n = 15$ images analyzed, with ~40,000-PSD95 immunoreactive puncta per image) and wild-type littermates ($n = 16$) (*t* test $t_{29} = 1.47$, $P = 0.15$). * $P < 0.05$, ns = not significant ($P > 0.05$). Data are presented as mean \pm s.e.m.



Changes in gene expression during memory consolidation

Together, these data indicate that reduced BAF53b function interferes substantially with the functional and structural foundations of long-term memory, that is, memory consolidation. Thus, we set out to identify which genes BAF53b regulates during memory consolidation. We performed an RNA sequencing experiment (Fig. 7) using dorsal hippocampal tissue from four groups of animals: *Baf53b*^{+/-} mice taken directly from their home cage without training, *Baf53b*^{+/-} mice taken 30 min after OLM training, wild-type mice taken directly from their home cage without training and wild-type mice taken 30 min after OLM training. All *Baf53b*^{+/-} and wild-type mice were handled and habituated as described for OLM (Fig. 2a and Supplementary Fig. 2). On the training day, half of the mice from each genotype were killed 30 min after OLM training. We have previously observed substantial gene expression changes in the dorsal hippocampus 30 min after OLM training²⁸. Mean PHRED quality scores indicate high-quality sequencing data for each replicate (Supplementary Fig. 6a). After mapping and considering the haploid genome^{29,30}, RNA sequencing successfully covered transcriptome 298.50 times (Supplementary Fig. 6b) and significant differences in expression profiles were examined between all pairs of samples for $P < 0.05$ (refs. 31–33).

We first compared the expression profiles of the wild-type and *Baf53b*^{+/-} mice home cage groups and found that the majority of genes (19,524) were equivalently expressed at baseline in the two groups (Fig. 7a). There were also groups of genes that showed increased expression (80) in wild-type compared with *Baf53b*^{+/-} mice and vice versa (57) at home cage (Supplementary Tables 1 and 2). We next examined differences in gene expression following training in the wild-type mice. Consistent with numerous studies³⁴, wild-type mice showed robust changes in gene expression, including many immediate early genes (IEGs), following OLM training (compared with home cage; Fig. 7b and Supplementary Tables 3 and 4), indicating that the training period was sufficient to induce activity-dependent gene expression during memory consolidation. In addition, many of the activity-regulated genes (124) increased in the wild type were also significantly induced in *Baf53b*^{+/-} mice following training

($P < 0.05$; Supplementary Table 5). These genes were enriched for Gene Ontology^{35–38} terms for regulation of transcription, RNA processing and intracellular signaling, and included the majority of IEGs (Fig. 7c,d and Supplementary Table 6). This suggests that BAF53b and nucleosome remodeling do not affect IEG expression during memory consolidation and that the long-term memory impairments observed in *Baf53b*^{+/-} mice are caused by different mechanisms. Of the 300 genes with increased expression in the wild type following OLM training, the expression of 176 failed to significantly increase in the *Baf53b*^{+/-} mice ($P > 0.05$; Fig. 7b and Supplementary Table 7). These genes were enriched for Gene Ontology terms involving transcription regulation and neurogenesis, as well as chromosome organization and chromatin modification, indicating a potential role for BAF53b in organizing higher order chromatin structure. In the *Baf53b*^{+/-} mice, there were also a group of genes (171) that were induced following behavior that were not normally increased in the wild type (Fig. 7b and Supplementary Table 8). These genes were enriched for Gene Ontology terms involving regulation of cell death, glutamate release, behavioral response to drugs of abuse, synaptic transmission and regulation of neurogenesis.

In addition to increases in gene expression, there were 101 genes whose expression decreased in the wild type following OLM training compared with home cage (Fig. 7b) and 76 genes that decreased in the *Baf53b*^{+/-} mice. Of the 101 genes that decreased in the wild type, 14 also decreased in the *Baf53b*^{+/-} mice (Supplementary Table 9) and 87 that did not (Supplementary Table 10). The 87 genes that failed to show an activity-dependent decrease in expression in the *Baf53b*^{+/-} mice were enriched for Gene Ontology terms involving cell homeostasis, postsynaptic cell membrane and cytoskeleton. In addition to the impaired decrease in gene expression, the *Baf53b*^{+/-} mice also had 62 genes whose decrease in expression following behavior was not matched in the wild type (Supplementary Table 11). These aberrantly decreased genes were enriched for Gene Ontology terms involving mitochondria function.

To further explore the link between the impairments in maintenance of long-term potentiation and cofilin phosphorylation,

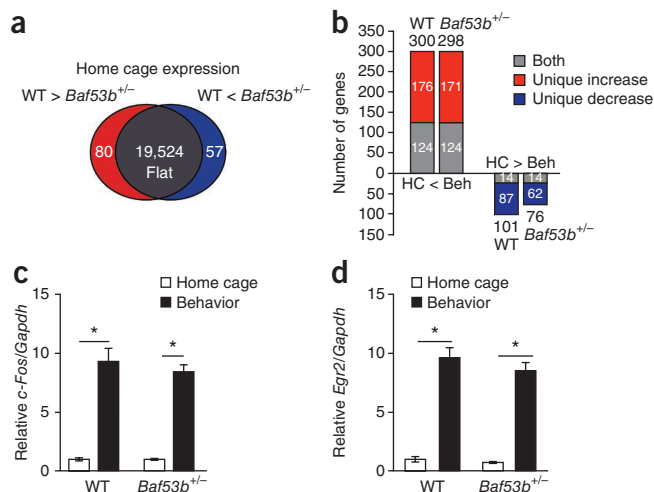


Figure 7 Differential gene expression in *Baf53b*^{+/-} mice by RNA sequencing. **(a)** Gene expression diagram for wild-type compared with *Baf53b*^{+/-} mice taken directly from the home cage. **(b)** Gene expression for genes that increased or decreased expression following behavior (30 min post training) compared with home cage. Genes with differential expression at home cage were removed before analysis. ‘Both’ indicates genes regulated similarly in wild-type and *Baf53b*^{+/-} mice. ‘Unique Increase’ comprises genes that increased in only the indicated genotype. ‘Unique Decrease’ comprises genes that decreased in only the indicated genotype. Groups: *Baf53b*^{+/-} mice taken from home cage (HC, *n* = 6), *Baf53b*^{+/-} mice taken 30 min post training (Beh, *n* = 6), wild-type taken from home cage (*n* = 6) and wild-type taken 30 min post training (*n* = 6). Total gene counts for each genotype given above or below each column. **(c)** qRT-PCR validation of the IEG *c-Fos* (ANOVA; main effect of behavior, $F_{1,20} = 157.6$, $P < 0.0001$; no effect of genotype, $F_{1,20} = 0.49$, $P = 0.49$; no interaction, $F_{1,20} = 0.45$, $P = 0.51$). Expression is shown relative to *Gapdh* and normalized to wild-type mice taken from home cage. **(d)** qRT-PCR validation of the IEG *Egr2* (ANOVA; main effect of behavior, $F_{1,20} = 224.2$, $P < 0.0001$; no effect of genotype, $F_{1,20} = 1.53$, $P = 0.23$; no interaction, $F_{1,20} = 0.55$, $P = 0.47$). Expression is shown relative to *Gapdh* and normalized to wild-type mice taken from home cage. * $P < 0.05$, *n* values refer to number of mice.

we examined gene expression for Gene Ontology terms involved in actin cytoskeleton and the postsynaptic density. Most genes examined showed similar expression between the *Baf53b*^{+/-} mice and their wild-type littermates. However, there were several genes that showed misregulation either at baseline (home cage) or following OLM training that are involved in regulating the Rac-PAK and RhoA-LIMK pathways that both culminate in phosphorylation of cofilin and actin cytoskeleton reorganization²³ (**Supplementary Table 12**). For example, *mir132* has been shown to regulate spine plasticity^{39,40} and long-term OLM⁴¹ by regulating Rac1 activity through translational repression of p250GAP³⁹. Additional regulators of this pathway were also disrupted in the *Baf53b*^{+/-} mice, including *Citron* (Rho interacting kinase) and *Fhl2* (a member of the four-and-a-half LIM only protein family implicated in linking signaling pathways to transcriptional regulation). Components upstream of the Rac-PAK and RhoA-LIMK were also altered in the *Baf53b*^{+/-} mice, including the NMDA receptor subunits *Grin2b* and *Grin2a*, as well as *EfnA4*.

DISCUSSION

Epigenetic mechanisms of gene regulation are emerging as a critical mechanism underlying long-term memory processes. The majority of the evidence supporting this idea comes from examination of chromatin modification (for example, histone acetylation) and DNA

methylation. However, nucleosome remodeling, which represents a third major epigenetic mechanism involved in regulating gene expression that has been shown to work together with chromatin modification and DNA methylation in yeast and cancer research, has yet to be investigated with regard to cognitive function. It has become increasingly important to understand the role of nucleosome remodeling considering the recent studies showing that mutations in the BAF complex are associated with intellectual disability disorders in humans^{12–14}. We found that both a dominant-negative and heterozygous knockout of BAF53b produced severe long-term memory and LTP consolidation impairments, providing, to the best of our knowledge, the first evidence that nucleosome remodeling is critical for synaptic plasticity and memory. Reintroduction of BAF53b into dorsal hippocampus using adeno-associated virus rescued long-term memory deficits in the *Baf53b*^{+/-} mice, providing clear evidence for the role of BAF53b in memory formation in the adult, independent of its role in neuronal development. The rescue effect was specific to the hippocampus-dependent OLM task, further supporting a specific role for BAF53b in adult memory formation.

The transgenic approach allowed us to avoid potential effects of expressing mutant *BAF53bΔHD* on embryonic development, but the heterozygous knockout mice did not appear to have observable developmental defects either. Both genetically modified mice exhibited severe impairments in long-term memory for hippocampus-dependent tasks (object location and contextual fear conditioning). In contrast, long-term memory for cued fear was normal in both *Baf53b*^{+/-} and *BAF53bΔHD*^{low} lines. This suggests that the hippocampus may be more sensitive to alterations in BAF53b function, as cued fear memory is considered to be hippocampus independent. BAF53b may also have a role in cortex-dependent long-term memory, as mutant BAF53b mice also exhibited impaired long-term memory for object recognition. When performed in this manner, the task mainly depends on the perirhinal and insular cortices, indicating a potential role for BAF53b-mediated gene expression in these cortical regions.

The observed long-term memory impairments were associated with specific hippocampal LTP deficits and altered dendritic spine morphology. In general, BAF53b appeared to be necessary for LTP consolidation, as induction and initial expression of potentiation were normal. However, we did observe substantially increased initial potentiation in the *BAF53bΔHD*^{high} line, which then showed a failure to stabilize that was similar to that of the *BAF53bΔHD*^{low} and *Baf53b*^{+/-} lines. Notably, the more severe LTP phenotype in the *BAF53bΔHD*^{high} mice compared with the *BAF53bΔHD*^{low} and *Baf53b*^{+/-} mice suggests that higher transgene expression alters the degree to which BAF53b effects induction, initial expression and consolidation of LTP. Given recent findings that mutations in subunits of the mammalian BAF complex are linked with sporadic autism, sporadic mental retardation and syndromic intellectual disability^{12–16}, the spectrum of synaptic plasticity and memory impairments found with our different manipulations of BAF53b could serve as a model for disorders such as Coffin-Siris and Nicolaides-Baraitser syndrome^{12–14}, and intellectual disability in general.

Notably, the impaired long-term memory and LTP consolidation deficits were associated with altered spine dynamics in the adult *Baf53b*^{+/-} mice following TBS. It is generally considered that pCofilin marks spines undergoing activity-dependent actin reorganization and that an expansion in spine size underlies the maintenance of LTP^{24,42}. Similarly, *BAF53bΔHD*^{high} mice had reduced availability of thin spines, consistent with the postsynaptic impairments in long-term synaptic plasticity. In juvenile and mature hippocampus, it is generally considered that thin spines are those in which afferent-patterned

stimulation induces structural and functional plasticity, leading to incorporation of AMPA-type glutamate receptor in the synapse and a conversion from a thin to a mushroom-type spine^{8,24,25,43}. The specific loss of thin spines may indicate a loss in the ability to respond to afferent-patterned stimulation by functional and structural plasticity, namely, incorporation of AMPA-type glutamate receptor in the synapse, synapse growth and the conversion of a thin to a mushroom type spine^{24–27,43}. Given that these spine changes occurred relatively early in life (by 3 weeks of age), they may contribute to the more severe LTP phenotype observed in *BAF53bΔHD^{high}* mice, more closely mimicking the deficits observed in individuals with intellectual disability.

The RNA sequencing data indicates that spine abnormalities may be a result of altered BAF53b-mediated gene expression. In the *Baf53b^{+/-}* mice, several key postsynaptic density genes involved in spine plasticity showed altered expression, including multiple regulators of the Rac-PAK and RhoA-LIMK pathways. For example, *mir132* expression was increased following OLM training in wild-type mice, but not in *Baf53b^{+/-}* mice. *mir132* has been shown to regulate spine plasticity^{39,40} and long-term OLM⁴¹ by regulating Rac1 activity through translational repression of p250GAP³⁹. *mir132* also blocks the translation of methyl CpG-binding protein 2 (MeCP2)⁴⁴, a transcriptional repressor that interacts with methylated DNA. *Mecp2* mutant mice have impairments in synaptic plasticity and a variety of behaviors, including long-term memory formation (for a review, see ref. 45), indicating that MeCP2 is critical for normal brain function. In humans, mutations in MeCP2 have been linked to Rett syndrome, a developmental disorder characterized by cognitive deficits similar to autism⁴⁶. In addition to *mir132*, *Baf53b^{+/-}* mice had alterations in gene expression of other regulators of the Rac-PAK and RhoA-LIMK pathways, both at the level of the postsynaptic density (*Grin2b* and *Grin2a* and *Efna4*) and at the level of pathway regulation (*Citron* and *Fhl2*). Understanding how exactly BAF53b and the nBAF complex is involved in the regulation of these and other genes will be critical, especially considering that spine abnormalities appear to be a common feature in intellectual disabilities, including nonsyndromic intellectual disability, Down, Fragile X and Rett syndromes⁴⁷.

In the transgenic mice, we targeted a hydrophobic domain of BAF53b. Further analysis will be necessary to fully understand how deletion of the hydrophobic domain impairs nBAF-mediated nucleosome remodeling. Nucleosome remodeling experiments are almost exclusively carried out *in vitro* and in cell culture, but nucleosome positioning experiments using high-density sequencing are emerging, which may make this more feasible in heterogeneous cell populations of various brain regions associated with learning and memory. In addition, currently available antibodies are insufficient to perform a chromatin immunoprecipitation, making the localization of BAF53b to specific DNA binding sites unfeasible. It is also unclear how neuronal activity induced by a learning event activates nBAF-mediated nucleosome remodeling. In cultured neurons, nBAF interacts with the calcium-regulated transcriptional activator calcium-response transactivator (CREST)⁸. Calcium influx activates CREST-mediated transcription, which is required for normal activity-dependent dendritic development^{48,49}. *In vitro*, BAF53b is not required for the CREST-nBAF interaction, but loss of BAF53b does disrupt localization of both nBAF and CREST to target gene promoters⁸. CREST expression in the hippocampus continues into adulthood⁴⁸ and may serve as a potential mechanism to link neuronal activity to nBAF-mediated nucleosome remodeling.

In summary, recent studies have shown that mutations in various subunits of the BAF complex cause intellectual disability disorders in humans^{12–17} and studies in culture have shown that BAF53b,

in particular, is necessary for dendritic outgrowth⁸. However, there has been no clear evidence linking BAF-mediated nucleosome remodeling to cognition. We found for the first time, to the best of our knowledge, that nBAF is necessary for synaptic plasticity and long-term memory processes, likely via the regulation of gene expression required for spine structure and function. These findings support the overall idea that impaired nucleosome remodeling may be an important underlying mechanism for intellectual disability disorders.

METHODS

Methods and any associated references are available in the [online version of the paper](#).

Note: Supplementary information is available in the online version of the paper.

Accession codes. RNA sequencing data have been deposited in NCBI's Gene Expression Omnibus⁵⁰ and are accessible through GEO Series accession number [GSE44229](#).

ACKNOWLEDGMENTS

We wish to acknowledge the University of California at Irvine Institute for Genomics and Bioinformatics and Genomics High-Throughput Facility, and J. Hayes for additional computing support. We would like to thank J. Guzowski and T. Miyashita for their technical expertise and the use of the BX61 microscope and XC10 camera. This work was supported by grants from the US National Institutes of Health (MH081004 and DA025922 to M.A.W., and training grant T32-AG00096-29 to A.V.C.). G.L., E.K. and Y.J. were supported by grants from the US National Institutes of Health (P01 NS045260) and ONR (#N00014-10-1-0072). T.Z.B. was supported by US National Institutes of Health grants NS 28912 and MH73136. The work of M.Z., C.M. and P.B. was supported by grants from the National Science Foundation (IIS-0513376), the US National Institutes of Health (LM010235) and the National Library of Medicine (T15 LM07443) to P.B.

AUTHOR CONTRIBUTIONS

A.V.-C., D.P.M., R.M.B. and M.A.W. designed the experiments. A.V.-C., D.P.M. and R.M.B. conducted the experiments. A.V.-C. and M.A.W. wrote the manuscript. E.K. and Y.J. conducted the electrophysiological experiments and analyzed the results. A.B. conducted and analyzed the pCofilin experiments. Y.C. and T.Z.B. designed and conducted the spine analysis. C.N.M., M.Z. and P.B. performed the RNA sequencing analysis. S.A., A.S., J.H., A.T., R.D. and R.J.P. performed the behavioral experiments. M.C. made the AAV-*hrGFP* virus. J.I.W. and G.R.C. provided technical assistance and assisted in manuscript preparation. P.B., T.Z.B. and G.L. assisted in experimental design, data analysis and manuscript preparation.

COMPETING FINANCIAL INTERESTS

The authors declare no competing financial interests.

Reprints and permissions information is available online at <http://www.nature.com/reprints/index.html>.

- Day, J.J. & Sweatt, J.D. Cognitive neuroepigenetics: a role for epigenetic mechanisms in learning and memory. *Neurobiol. Learn. Mem.* **96**, 2–12 (2011).
- Zahir, F.R. & Brown, C.J. Epigenetic impacts on neurodevelopment: pathophysiological mechanisms and genetic modes of action. *Pediatr. Res.* **69**, 92R–100R (2011).
- Hargreaves, D.C. & Crabtree, G.R. ATP-dependent chromatin remodeling: genetics, genomics and mechanisms. *Cell Res.* **21**, 396–420 (2011).
- Wu, J.I., Lessard, J. & Crabtree, G.R. Understanding the words of chromatin regulation. *Cell* **136**, 200–206 (2009).
- Wang, W. *et al.* Purification and biochemical heterogeneity of the mammalian SWI-SNF complex. *EMBO J.* **15**, 5370–5382 (1996).
- Olave, I., Wang, W., Xue, Y., Kuo, A. & Crabtree, G.R. Identification of a polymorphic, neuron-specific chromatin remodeling complex. *Genes Dev.* **16**, 2509–2517 (2002).
- Zhao, K. *et al.* Rapid and phosphoinositide-dependent binding of the SWI/SNF-like BAF complex to chromatin after T lymphocyte receptor signaling. *Cell* **95**, 625–636 (1998).
- Wu, J.I. *et al.* Regulation of dendritic development by neuron-specific chromatin remodeling complexes. *Neuron* **56**, 94–108 (2007).
- Lessard, J. *et al.* An essential switch in subunit composition of a chromatin remodeling complex during neural development. *Neuron* **55**, 201–215 (2007).
- Yoo, A.S., Staahl, B.T., Chen, L. & Crabtree, G.R. MicroRNA-mediated switching of chromatin-remodeling complexes in neural development. *Nature* **460**, 642–646 (2009).

11. Yoo, A.S. *et al.* MicroRNA-mediated conversion of human fibroblasts to neurons. *Nature* **476**, 228–231 (2011).
12. Tsurusaki, Y. *et al.* Mutations affecting components of the SWI/SNF complex cause Coffin-Siris syndrome. *Nat. Genet.* **44**, 376–378 (2012).
13. Santen, G.W.E. *et al.* Mutations in SWI/SNF chromatin remodeling complex gene *ARID1B* cause Coffin-Siris syndrome. *Nat. Genet.* **44**, 379–380 (2012).
14. Van Houdt, J.K. *et al.* Heterozygous missense mutations in *SMARCA2* cause Nicolaides-Baraitser syndrome. *Nat. Genet.* **44**, 445–449 (2012).
15. Halgren, C. *et al.* Corpus callosum abnormalities, intellectual disability, speech impairment, and autism in patients with haploinsufficiency of *ARID1B*. *Clin. Genet.* **82**, 248–255 (2012).
16. Hoyer, J., Ekici, A.B., Endeke, S., Popp, B. & Zweier, C. Haploinsufficiency of *ARID1B*, a member of the SWI/SNF-A chromatin-remodeling complex, is a frequent cause of intellectual disability. *Am. J. Hum. Genet.* **90**, 565–572 (2012).
17. Neale, B.M. *et al.* Patterns and rates of exonic *de novo* mutations in autism spectrum disorders. *Nature* **485**, 242–245 (2012).
18. Park, J., Wood, M.A. & Cole, M.D. BAF53 forms distinct nuclear complexes and functions as a critical c-Myc-interacting nuclear cofactor for oncogenic transformation. *Mol. Cell Biol.* **22**, 1307–1316 (2002).
19. Mayford, M. *et al.* Control of memory formation through regulated expression of a CaMKII transgene. *Science* **274**, 1678–1683 (1996).
20. Kojima, N. *et al.* Rescuing impairment of long-term potentiation in *fyn*-deficient mice by introducing *Fyn* transgene. *Proc. Natl. Acad. Sci. USA* **94**, 4761–4765 (1997).
21. Larson, J., Wong, D. & Lynch, G. Patterned stimulation at the theta frequency is optimal for the induction of hippocampal long-term potentiation. *Brain Res.* **368**, 347–350 (1986).
22. Lauterborn, J.C. *et al.* Brain-derived neurotrophic factor rescues synaptic plasticity in a mouse model of fragile X syndrome. *J. Neurosci.* **27**, 10685–10694 (2007).
23. Rex, C.S. *et al.* Different Rho GTPase-dependent signaling pathways initiate sequential steps in the consolidation of long-term potentiation. *J. Cell Biol.* **186**, 85–97 (2009).
24. Chen, L.Y., Rex, C.S., Casale, M.S., Gall, C.M. & Lynch, G. Changes in synaptic morphology accompany actin signaling during LTP. *J. Neurosci.* **27**, 5363–5372 (2007).
25. Bourne, J.N. & Harris, K.M. Balancing structure and function at hippocampal dendritic spines. *Annu. Rev. Neurosci.* **31**, 47–67 (2008).
26. Grutzendler, J., Kasthuri, N. & Gan, W.B. Long-term dendritic spine stability in the adult cortex. *Nature* **420**, 812–816 (2002).
27. Harris, K.M., Jensen, F.E. & Tsao, B. Three-dimensional structure of dendritic spines and synapses in rat hippocampus (CA1) at postnatal day 15 and adult ages: implications for the maturation of synaptic physiology and long-term potentiation. *J. Neurosci.* **12**, 2685–2705 (1992).
28. Barrett, R.M. *et al.* Hippocampal focal knockout of CBP affects specific histone modifications, long-term potentiation and long-term memory. *Neuropsychopharmacology* **36**, 1545–1556 (2011).
29. Fujita, P.A. *et al.* The UCSC Genome Browser database: update 2011. *Nucleic Acids Res.* **39**, D876–D882 (2011).
30. Langmead, B., Trapnell, C., Pop, M. & Salzberg, S.L. Ultrafast and memory-efficient alignment of short DNA sequences to the human genome. *Genome Biol.* **10**, R25 (2009).
31. Mortazavi, A., Williams, B.A., McCue, K., Schaeffer, L. & Wold, B. Mapping and quantifying mammalian transcriptomes by RNA-Seq. *Nat. Methods* **5**, 621–628 (2008).
32. Kayala, M.A. & Baldi, P. Cyber-T web server: differential analysis of high-throughput data. *Nucleic Acids Res.* **40**, W553–559 (2012).
33. Baldi, P. & Long, A.D. A Bayesian framework for the analysis of microarray expression data: regularized t-test and statistical inferences of gene changes. *Bioinformatics* **17**, 509–519 (2001).
34. Alberini, C.M. Transcription factors in long-term memory and synaptic plasticity. *Physiol. Rev.* **89**, 121–145 (2009).
35. Ashburner, M. *et al.* Gene ontology: tool for the unification of biology. The Gene Ontology Consortium. *Nat. Genet.* **25**, 25–29 (2000).
36. Ogata, H. *et al.* KEGG: Kyoto Encyclopedia of Genes and Genomes. *Nucleic Acids Res.* **27**, 29–34 (1999).
37. Kanehisa, M., Goto, S., Sato, Y., Furumichi, M. & Tanabe, M. KEGG for integration and interpretation of large-scale molecular data sets. *Nucleic Acids Res.* **40**, D109–D114 (2012).
38. Dennis, G. *et al.* DAVID: Database for Annotation, Visualization and Integrated Discovery. *Genome Biol.* **4**, 3 (2003).
39. Wayman, G.A. *et al.* An activity-regulated microRNA controls dendritic plasticity by down-regulating p250GAP. *Proc. Natl. Acad. Sci. USA* **105**, 9093–9098 (2008).
40. Impey, S. *et al.* An activity-induced microRNA controls dendritic spine formation by regulating Rac1-PAK signaling. *Mol. Cell Neurosci.* **43**, 146–156 (2010).
41. Hansen, K.F., Sakamoto, K., Wayman, G.A., Impey, S. & Obrietan, K. Transgenic *miR132* alters neuronal spine density and impairs novel object recognition memory. *PLoS ONE* **5**, e15497 (2010).
42. Fedulov, V. *et al.* Evidence that long-term potentiation occurs within individual hippocampal synapses during learning. *J. Neurosci.* **27**, 8031–8039 (2007).
43. Fukazawa, Y. *et al.* Hippocampal LTP is accompanied by enhanced F-actin content within the dendritic spine that is essential for late LTP maintenance *in vivo*. *Neuron* **38**, 447–460 (2003).
44. Klein, M.E. *et al.* Homeostatic regulation of MeCP2 expression by a CREB-induced microRNA. *Nat. Neurosci.* **10**, 1513–1514 (2007).
45. Nelson, E.D. & Monteggia, L.M. Epigenetics in the mature mammalian brain: effects on behavior and synaptic transmission. *Neurobiol. Learn. Mem.* **96**, 53–60 (2011).
46. Amir, R.E. *et al.* Rett syndrome is caused by mutations in X-linked MECP2, encoding methylCpG-binding protein 2. *Nat. Genet.* **23**, 185–188 (1999).
47. Levenga, J. & Willemsen, R. Perturbation of dendritic protrusions in intellectual disability. *Prog. Brain Res.* **197**, 153–168 (2012).
48. Aizawa, H. Dendrite development regulated by CREST, a calcium-regulated transcriptional activator. *Science* **303**, 197–202 (2004).
49. Qiu, Z. & Ghosh, A. A calcium-dependent switch in a CREST-BRG1 complex regulates activity-dependent gene expression. *Neuron* **60**, 775–787 (2008).
50. Edgar, R., Domrachev, M. & Lash, A.E. Gene Expression Omnibus: NCBI gene expression and hybridization array data repository. *Nucleic Acids Res.* **30**, 207–210 (2002).

ONLINE METHODS

Mice. All mice were between 8 and 15 weeks old at the time of behavioral testing. Mice had free access to food and water and lights were maintained on a 12:12-h light/dark cycle, with all behavioral testing performed during the light portion of the cycle. All experiments were conducted according to US National Institutes of Health guidelines for animal care and use and were approved by the Institutional Animal Care and Use Committee of the University of California, Irvine. All mice were group housed and backcrossed at least five generations to C57BL/6 mice (Jackson Labs).

Object location and novel object recognition tasks. Object location and object recognition were performed as previously described^{28,51}. Prior to training, mice are handled 1–2 min for 5 d and then habituated to the experimental apparatus for 5 min d⁻¹ for 4–6 d in the absence of objects. During the training period, mice were placed into the experimental apparatus with two identical objects (100-ml beakers or light bulbs or vases) and allowed to explore for 10 min⁵¹. During the retention test (24 h for long-term memory or 90 min for short-term memory), mice were allowed to explore the experimental apparatus for 5 min. Exploration was scored when a mouse's head was oriented toward the object within a distance of 1 cm or when the nose was touching the object. The relative exploration time (*t*) was recorded and expressed as a discrimination index ($DI = (t_{\text{novel}} - t_{\text{familiar}}) / (t_{\text{novel}} + t_{\text{familiar}}) \times 100\%$). Mean exploration times were then calculated and the discrimination indexes between treatment groups compared. Mice that explored both objects for less than 3 s in total during either training or testing were removed from further analysis. Mice that demonstrated an object preference during training ($DI > \pm 20$) were also removed.

Elevated plus maze. The plus-maze consisted of two open arms, 30 × 5 cm, and two enclosed arms, 30 × 5 × 15 cm. The arms extended from a 5 × 5 cm central platform, and the apparatus was raised to a height of 40 cm above the floor. The light level was adjusted to 15 lux. Testing (5 min) consisted of placing a mouse onto the central platform of the maze facing an open arm. Between subjects, the maze was cleaned with 70% ethanol. The percentage of time spent in the closed and open arms was scored using EthoVision 3.1 (Noldus Information Technology).

Fear conditioning. Contextual and cued fear conditioning were performed as previously described^{28,51,52}. For contextual fear conditioning, a single 2-s, 0.70-mA scrambled foot shock was given at time 2:28 of a 3-min training period followed by a 5-min testing period 24 h later. For cued fear conditioning, mice were in the chamber for 2 min, followed by a 30-s tone that co-terminated with a 2-s, 0.70-mA scrambled foot shock. Mice were allowed to remain in the chamber for an additional 30 s. Mice were tested in a novel context (2 min) 24 h after conditioning, followed by a 3-min tone. Freezing behavior was measured using EthoVision 3.1 (Noldus Information Technology)⁵¹.

pCofilin analysis. Hippocampal slices were prepared as described below. Following a baseline recording, slices were either given control stimulation (three pulses per min) or ten theta burst stimulation. All the slices were collected 7 min after stimulation and placed into cold 4% paraformaldehyde (wt/vol). As previously described⁵³, hippocampal slices were subsection of a freezing microtome and slide mounted. Immunocytochemical labeling was done by washing slices with 0.1 M phosphate buffer, then placed in a cocktail of primary antibodies to pCofilin (ABCam, AB12866; 1:250) and PSD95 (ThermoScientific, MA1-045, 1:800) in diluent that included 0.1 M phosphate buffer, 0.3% Triton X-100 (vol/vol) and 1.8% bovine serum albumin (wt/vol). Sections were exposed to primary antibody for two nights at 4 °C. Tissue was then rinsed three times with 0.1 M PB and incubated in secondary antibodies for donkey antibody to mouse Alexa Fluor 488 (1:1,000, Life Technologies, A-21202) and donkey antibody to rabbit Alexa Fluor 594 (1:1,000, Life Technologies, A-2107).

Imaging and quantification were completed as described previously⁵³. Briefly, images were acquired on a Leica DM6000B using a 63× Plan Apo objective (1.4 numerical aperture). Image acquisition and deconvolution (99% confidence) were done using Volocity 6.0 (Perkin-Elmer), at which point deconvolved images were exported and quantified using previously described in-house analysis software.

Spine analysis. Immunohistochemistry was carried out on 20-μm free-floating sections from perfused, fixed brains as described previously^{28,51}. Mouse antibody

to GFP (1:8,000, G6539, Sigma) and antibody to mouse IgG conjugated to Alexa Fluor 488 (1:200, 948490, Molecular Probes) were used. Sections from all experimental groups were run concurrently in the same conditions, and analyzed without knowledge of treatment group. The analysis was performed as previously described⁵⁴.

Immunohistochemistry. Immunofluorescence was carried out on fresh frozen 20-μm thaw-mounted sections using the Tyramide Signal Amplification (TSA) Plus system (Perkin Elmer, NEL704A001KT). Briefly, slides were fixed in 4% paraformaldehyde (10 min), permeabilized in 0.01% Triton X-100 in 0.1 M PBS (5 min), and incubated in 2% hydrogen peroxide diluted in 0.1 M PBS (vol/vol) (15 min). All slides were then blocked (1 h) using the TSA blocking buffer, incubated overnight (4 °C) in rabbit antibody to BAF53b (1:500, generous gift from G.R.C.) and/or mouse antibody to NeuN (1:1,000, MAB377, Millipore), washed (3 × 5 min in 0.1 M PBS with 0.05% Tween-20, vol/vol), and incubated for 1 h at 21–23 °C with FITC-conjugated goat antibody to mouse IgG (1:1,000, Millipore Bioscience Research Reagents) or HRP-conjugated donkey antibody to rabbit IgG (1:1,000, 711-036-152, Jackson ImmunoResearch). Slides were again washed and the TSA reaction was performed to detect BAF53b as described in the kit (TSA-CY3 1:50). Slides were coverslipped in ProLong Gold antifade reagent with DAPI (P-36931, Invitrogen).

Crestyl violet and Luxol Blue staining. Mice were transcardially perfused with saline (2 min) followed by 4% paraformaldehyde (10 min). Brains were post-fixed overnight (4% paraformaldehyde) followed by 30% sucrose (wt/vol, 2 d) and then flash frozen. Luxol Blue and crestyl violet staining were performed as previously described⁵⁵. Briefly, free-floating sections (50 μm) were washed in 0.1 M phosphate-buffered saline (PBS, 3 × 10 min), 70% ethanol (2 × 5 min) and incubated in 70% ethanol overnight (21–23 °C). Sections were transferred to prewarmed Luxol Fast Blue solution (0.1% Luxol Fast Blue Solvent 38 (wt/vol, Sigma) dissolved in 96% ethanol and 10% acetic acid, vol/vol) and incubated overnight at 56 °C. Sections were washed sequentially (3 min) in water, 0.1 M PBS and lithium carbonate solution (0.05% lithium carbonate (wt/vol) in water). Sections were differentiated in 70% ethanol (3 min), washed twice (5 min) in 0.1 M PBS, mounted and dried overnight. The next day, sections were crestyl violet stained: defatting (30 min 50% chloroform/50% ethanol), dehydrations (100%, 95%, 70% and 50% ethanol sequentially), rinsed (water), crestyl violet stained (six dips), rehydrated (50%, 70%, 95%, 100% ethanol), cleared (Hemo-De) and coverslipped.

Western blot. Dorsal hippocampus was homogenized in RIPA buffer (Boston BioProducts, BP-115) with protease and phosphatase inhibitors (ThermoScientific, 1861281) using a dounce homogenizer. *Baf53b*^{-/-} brain tissue was collected from postnatal day 2 pups to verify antibody specificity. Protein lysates were quantified using a modified Bradford assay (BioRad, 500-0006). We loaded 10 μg of total protein lysate per lane on a 4–12% Bis Tris gel (Novex) and ran it for 50 min at 200 V. Blots were then transferred overnight at 15V at 4 °C on to 0.45-μm nitrocellulose membranes (Novex). Total protein transfer was verified using Ponceaus staining. Membranes were blocked in StartingBlock T20 (ThermoScientific, 37543) for 30 min and then probed with rabbit antibody to BAF53b (1:1,000, generous gift from G.R.C.). The membranes were washed (3 × 10 min in 0.1 M PBS with 0.05% Tween-20, vol/vol) and probed with HRP-conjugated donkey antibody to rabbit (1:10,000, Jackson ImmunoResearch, 711-036-152). The membranes were washed and developed using Pierce SuperSignal West Pico Chemiluminescent Substrate (Pierce, 34077). Multiple film exposures were used to verify linearity. Blots were washed and then reprobed with rabbit antibody to GAPDH (1:1,000, Santa Cruz Biotechnology, SC25778). Relative densities were taken from scanned film using ImageJ (US National Institutes of Health). All values were normalized to GAPDH expression levels.

Slice preparation and recording. Hippocampal slices were prepared as previously described²⁸ from *Baf53b*^{+/-}, *BAF53ΔHD*^{low}, *BAF53ΔHD*^{high} and wild-type mice (approximately 2 months of age). Transverse hippocampal slices (300 μm) through the mid-third of the septotemporal axis of the hippocampus were placed in an interface recording chamber containing preheated artificial cerebrospinal fluid consisting of 124 mM NaCl, 3 mM KCl, 1.25 mM KH₂PO₄, 1.5 mM MgSO₄, 2.5 mM CaCl₂, 26 mM NaHCO₃ and 10 mM D-glucose and maintained at 31 ± 1 °C. Slices were continuously perfused at a rate of

1.75–2 ml min⁻¹ while the surface was exposed to warm, humidified 95% O₂ / 5% CO₂. Recordings began after at least 2 h of incubation.

fEPSPs were recorded from CA1b stratum radiatum using a single glass pipette (2–3 MΩ). Bipolar stainless steel stimulation electrodes (25 μm in diameter, FHC) were positioned at two sites (CA1a and CA1c) in the apical Schaffer collateral–commissural projections to provide activation of separate converging pathways of CA1b pyramidal cells. Pulses were administered in an alternating fashion to the two electrodes at 0.03 Hz using a current that elicited a 50% maximal response. After establishing a stable baseline, LTP was induced by delivering five or ten theta bursts (each burst was four pulses at 100 Hz and bursts were separated by 200 ms). Data were collected and digitized by NAC 2.0 Neurodata Acquisition System (Theta Burst).

Slices used for whole-cell recordings were prepared as previously described^{23,56}. Briefly, slices were placed in a submerged recording chamber and continuously perfused at 2–3 ml min⁻¹ with oxygenated (95% O₂/5% CO₂) artificial cerebrospinal fluid at 32 °C. Whole-cell recordings were made with 3–5 MΩ recording pipettes filled with solution of the following composition: 130 mM potassium gluconate, 0.1 mM EGTA, 0.5 mM MgCl₂, 10 mM HEPES and 2 mM ATP (pH 7.25, 285 mOsm) using an Axopatch 200A amplifier (Molecular Devices). mEPSCs were recorded at a holding potential of –70 mV in the presence of tetrodotoxin (1 μM) and bicuculline (50 μM). Data were filtered at 2 kHz, digitized at 1–5 kHz, stored on a computer, and analyzed off-line using Mini Analysis Program (Synaptosoft), Origin (OriginLab) and pCLAMP 7 (Molecular Devices) software.

AAV production and infusion. The wild-type BAF53b was V5 tagged and cloned into the pAAV-IRES-hrGFP Vector (Agilent Technologies) under the CMV promoter. Adeno-associated virus (AAV) serotype 2/1 for AAV-*Baf53b* was purchased from Penn Vector Core (University of Pennsylvania). AAV-hrGFP serotype 2/1 was generated and viral titer was determined by quantitative PCR with primers specific to hrGFP⁵⁷. A titer of 10¹⁰–10¹³ genome copies μl⁻¹ was used for all injections.

As previously described, 2 weeks before the experiments, 1.0 μl of virus per hemisphere was infused bilaterally into the dorsal hippocampus (anterior-posterior 2.0 mm, medial-lateral ±1.5 mm, 1.5 mm dorsal-ventral from bregma) at a rate of 6 ml h⁻¹ (refs. 28,51). All infusions were confirmed by immunohistochemistry.

RNA sequencing. RNA was isolated from bilateral, dorsal hippocampus using the using RNeasy minikit (Qiagen, 74104). RNA quality was assessed by Bioanalyzer, and only samples with an RNA integrity number greater than 9 were included for analysis. cDNA libraries for each group were prepared as described in the TruSeq RNA Sample Preparation v2 Guide (Illumina). Briefly, 3 μg of total RNA from each mouse was used as starting material. The mRNA was purified with poly-T oligo-attached magnetic beads and heat fragmented. The first and second strand cDNA were then synthesized and purified. The ends were blunted and the 3' end was adenylated to prevent concatenation of the template during adaptor ligation. For each group, a unique adaptor set was added to the ends of the cDNA and the libraries were amplified by PCR. The quality of the library was assessed by Bioanalyzer and quantified using qRT-PCR with a standard curve prepared from a purchased sequencing library (Illumina). Samples were multiplexed so that each behavioral group was represented in each flow cell of the sequencer. We pooled 10 nM of each library together in four multiplex libraries and sequenced them on an IlluminaHiSeq 2000 instrument during a single-end 50 cycles sequencing run by the Genomics High-Throughput Facility at the University of California, Irvine. The resulting sequencing data for each library were post-processed to produce FastQ files, then demultiplexed and filtered using both Illumina software CASAVA 1.8.2 and in-house software. Control reads successfully aligned to the PhiX control genome or poor-quality reads failing Illumina's standard quality tests were removed from the following analyses. The quality of the remaining sequences was further assessed using the PHRED quality scores produced in real time during the base-calling step of the sequencing run (Supplementary Fig. 6a).

Alignment to the reference genome and transcriptome. The reads from each replicate experiment were separately aligned to the reference genome²⁹

and corresponding transcriptome using the short-read aligners ELAND v2e (Illumina) and Bowtie³⁰. Reads uniquely aligned by both tools to known exons or splice junctions with no more than two mismatches were included in the transcriptome. Reads uniquely aligned, but with more than two mismatches, or reads matching several locations in the reference genome, were removed from the analysis. The percentage of reads assigned to the reference genome and transcriptome using this protocol is reported for each group of replicates (Supplementary Fig. 6b) with the corresponding percentage of covered genes (Supplementary Fig. 6b).

Gene expression and differential analysis. Gene expression levels were directly computed from the read alignment results for each replicate in the different groups. Standard RPKM values³¹ (reads per kilobase of exon model per million mapped reads) were extracted for each gene covered by the sequencing data and each replicate used in this study.

Differential transcriptional analyses were performed using CyberT^{32,33} across each pair of groups: wild type taken from home cage or after 30 min of OLM training and *Baf53b*^{+/-} taken from home cage or after 30 min of OLM training. Additional control analyses were performed using CASAVA. For different threshold values, the corresponding number of genes predicted to be differentially regulated, upregulated or downregulated was examined. Enrichment for specific tissue expression, Gene Ontology terms³⁵ and KEGG pathways^{36,37} was assessed using DAVID³⁸.

qRT-PCR. qRT-PCR was performed as described previously^{28,51}. Tissue was collected from dissections of dorsal hippocampus and stored in RNALater (Invitrogen, AM7020) at –80 °C until processed. RNA was isolated using RNeasy minikit (Qiagen, 74104). cDNA was made from 500–1,000 ng of total RNA using the Transcriptor First Strand cDNA Synthesis kit (Roche Applied Sciences, 04379012001). Primers and probes were derived from the Roche Universal ProbeLibrary (Supplementary Table 13) and used for multiplexing in the Roche Light-Cycle 480 II machine (Roche Applied Sciences). All values were normalized to *Gapdh* expression levels. Analysis and statistics were performed using the Roche proprietary algorithms and REST 2009 software based on the Pfaffl method^{58,59}.

Statistical analysis. Statistical analysis was conducted as indicated in the text and figure legends using Prism (GraphPad). Parametric tests (*t* test or ANOVA) were used where assumptions of normality (Shapiro-Wilk) and equal variance (F test or Bartlett's test) were met and were replaced by nonparametric equivalents where appropriate (Mann Whitney U or Kruskal-Wallis). Main effects and interactions for all ANOVAs or Kruskal-Wallis tests are described in the text. The appropriate *post hoc* tests (Bonferroni or Dunn's) are listed for each condition examined. All *t* tests were two-tailed using a *P* value of 0.05.

- McQuown, S.C. *et al.* HDAC3 is a critical negative regulator of long-term memory formation. *J. Neurosci.* **31**, 764–774 (2011).
- Vecsey, C.G. *et al.* Histone deacetylase inhibitors enhance memory and synaptic plasticity via CREB:CBP-dependent transcriptional activation. *J. Neurosci.* **27**, 6128–6140 (2007).
- Babayan, A.H. *et al.* Integrin dynamics produce a delayed stage of long-term potentiation and memory consolidation. *J. Neurosci.* **32**, 12854–12861 (2012).
- Chen, Y. *et al.* Impairment of synaptic plasticity by the stress mediator CRH involves selective destruction of thin dendritic spines via RhoA signaling. *Mol. Psychiatry* published, online doi:10.1038/mp.2012.17 (13 March 2012).
- Geisler, S., Heilmann, H. & Veh, R.W. An optimized method for simultaneous demonstration of neurons and myelinated fiber tracts for delineation of individual trunco- and palliothalamic nuclei in the mammalian brain. *Histochem. Cell Biol.* **117**, 69–79 (2002).
- Colgin, L.L., Jia, Y., Sabatier, J.-M. & Lynch, G. Blockade of NMDA receptors enhances spontaneous sharp waves in rat hippocampal slices. *Neurosci. Lett.* **385**, 46–51 (2005).
- Lawlor, P.A. *et al.* Novel rat Alzheimer's disease models based on AAV-mediated gene transfer to selectively increase hippocampal Abeta levels. *Mol. Neurodegener.* **2**, 11 (2007).
- Pfaffl, M.W. A new mathematical model for relative quantification in real-time RT-PCR. *Nucleic Acids Res.* **29**, e45 (2001).
- Pfaffl, M.W. *et al.* Real-time RT-PCR quantification of insulin-like growth factor (IGF)-1, IGF-1 receptor, IGF-2, IGF-2 receptor, insulin receptor, growth hormone receptor, IGF-binding proteins 1, 2 and 3 in the bovine species. *Domest. Anim. Endocrinol.* **22**, 91–102 (2002).